

Predictive ab-initio study of optoelectronic and magnetic properties of BaDyO₃ new perovskite

A. Labdelli

Biotechnology Applied to Agriculture and Environmental Preservation Laboratory (L.B.A.A.P.E)
Higher School of Agronomy-Mostaganem-Algeria

*Corresponding author, abbes.labdelli@univ-mosta.dz.

Received date: Nov. 14, 2022; accepted date: March 20, 2023

Abstract

The full potential linear augmented plane wave (FP-LAPW) method based on density functional theory (DFT), is used to study the structural, optoelectronic and magnetic properties of BaDyO₃, in different phases: cubic (space group pm $\bar{3}$ m), Tetragonal (I4mcm), orthorhombic (Ibmm, pbmm and pnma) with both generalized gradient approximation (LSDA) as well as The DFT-D3 method who gives structural results very close to the experimental, and LSDA+U approaches, where U is on-site Coulomb interaction correction.. We have analyzed the structural parameters, total and partial densities of states. The results show a ferromagnetic ground state for BaDyO₃ in LSDA+U due to the strong hybridization effect between Dy-4f and Ba-4f states. The integer value of the total magnetic moment is one of the significance of the semiconductor nature of this material. Furthermore, the results obtained, make the orthorhombic BaDyO₃ a promising candidate for application in spintronic.

Keywords: FP-LAPW; mBJ; G-type antiferromagnetic; Orthorhombic; Electronic structure; LSDA+U.

1. Introduction

Recently perovskites oxides have attracted enormous attentions because of their efficient use in ferroelectricity [1, 2], piezoelectricity [3, 4], high temperature super conductors, chemical reactors, gas separation membranes, solid state fuel cells, optoelectronic devices magnetoelectronic technologies [5, 6] and in spintronic domains [7, 8].

In this article, we investigate electronic structure and magnetic properties of the orthorhombic Perovskite oxide BaDyO₃, Based on first principle calculations. These properties are evaluated by using LSDA, LSDA+U (this approximation was used also by A. Labdelli et al. [9]) and mBJ approximations, where U is Hubbard parameter for considering the Coulomb repulsion between the highly localized 4f electrons.

It is important to notice that there are no theoretical and experimental data available for BaDyO₃ compound and this is why, we are motivated to study this material theoretically.

2. Method of calculation

In this work, we performed the calculations using the code WIEN2k [10, 11]. It is based on the full potential linearized augmented plane wave method (FP LAPW) [12].

Is that uses the Kohn-Sham equations [13], which are solved to calculate the structural, electronic and magnetic properties of the orthorhombic perovskite BaDyO₃.

In this method wave functions, charge density, and potential are expanded in spherical harmonics within nonoverlapping muffin-tin (MT) spheres, and plane waves are used in the remaining interstitial region of the unit cell. In the code, the core and valence states are treated differently. Core states are treated within a multi configuration relativistic Dirac-Fock approach, while valence states are treated in a scalar relativistic approach. The exchange-correlation energy, E_c was calculated using the Perdew-Wang LSDA[14] and the LSDA+U [15].

Very carefully, step analysis is done to ensure convergence of the total energy in terms of the variation cutoff-energy parameter. At the same time, we have used an appropriate set of k-points to compute the total energy. We compute equilibrium lattice constants and bulk moduli by fitting the total energy versus volume to the Murnaghan equation [15]. The standard built-in basis functions were applied with the valence configurations of (Ba: [Xe] 6s²), (Dy: [Xe]4f⁸) [16], and (O: 1s²2s²2p⁴). Basis functions were expanded as combinations of spherical harmonic functions inside non-overlapping spheres around the atomic sites (MT spheres) and in Fourier series in the interstitial

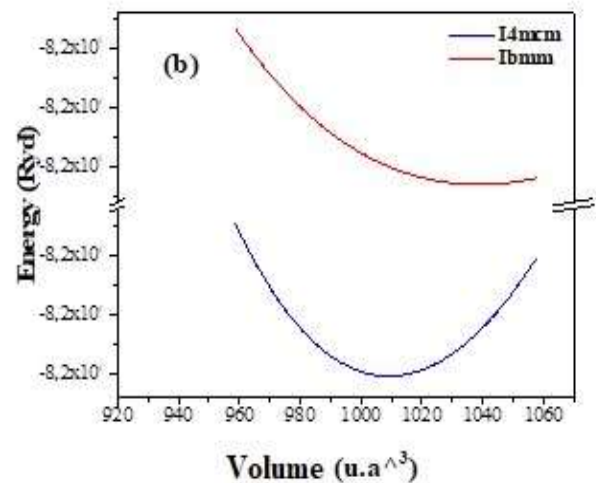
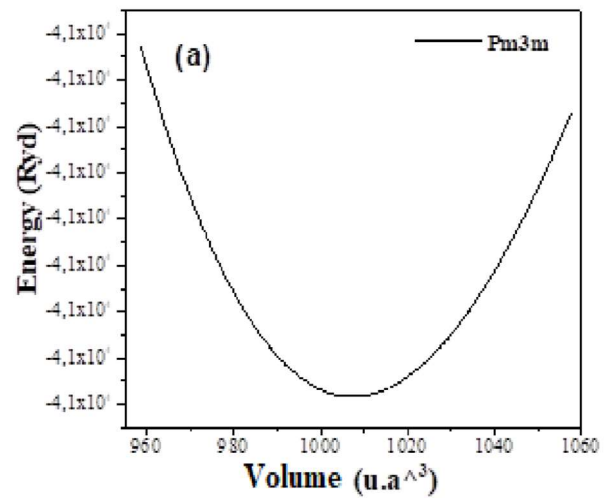
region. The valence wave functions, inside the spheres are expanded up to $l_{max}=10$. Reciprocal space integration is carried out with a k mesh of $(6 \times 4 \times 6)$, giving rise to 200 k -points. The wave functions in the interstitial region were expanded in plane waves with a cut-off of $k_{max} \cdot R_{MT}=8$. The muffin-tin (MT) radii of Ba, Dy and O were chosen to be 2.3, 2.02 and 1.79 Bohr, respectively. The lattice constants and bulk modulus are calculated by fitting the total energy versus volume according to the Murnaghan's equation of state [16]. For the exchange correlation functional, we have used the LSDA [12] as well as the DFT-D3 method who gives structural results very close to the experimental [17]. The magnetic ordering is studied using $2 \times 2 \times 2$ supercells to model the antiferromagnetic (AFM) configurations.

3. Results and discussions

3.1. Structural properties

To determine the structural constants such as equilibrium lattice constant and the bulk modulus for the compound $BaDyO_3$, We chose three systems. Cubic (with space group $Pm\bar{3}m$), tetragonal with space group $I4/mcm$ and orthorhombic with space group $Ibmm$, $Pnma$ and $Pbnm$. For that we used as reference materials $BaTbO_3$ [18, 19], to find the most stable structure, we performed the structural optimization by minimizing the total energy with respect to the cell parameters and the atomic position, $BaDyO_3$ assumes an orthorhombic structure with space group

points in the irreducible Brillouin zone, which is found to be sufficient to achieve convergence.



(b) tetragonal ($I4/mcm$) (c) orthorhombic ($Ibmm$), (d) orthorhombic ($Pbnm$), (e) orthorhombic ($Pnma$)

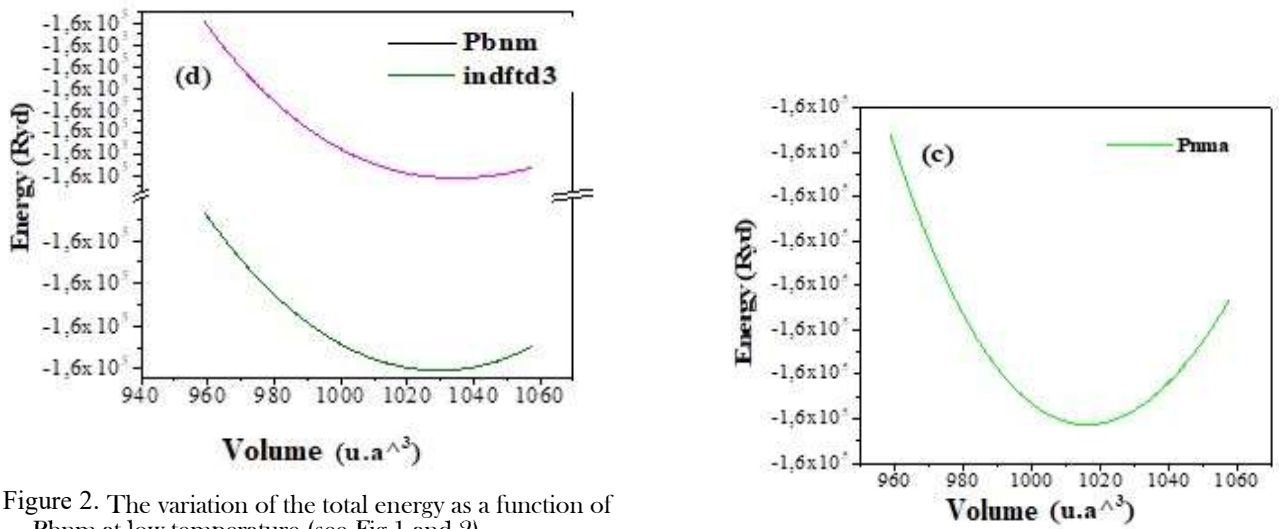


Figure 2. The variation of the total energy as a function of Pbnm at low temperature (see Fig.1 and 2).

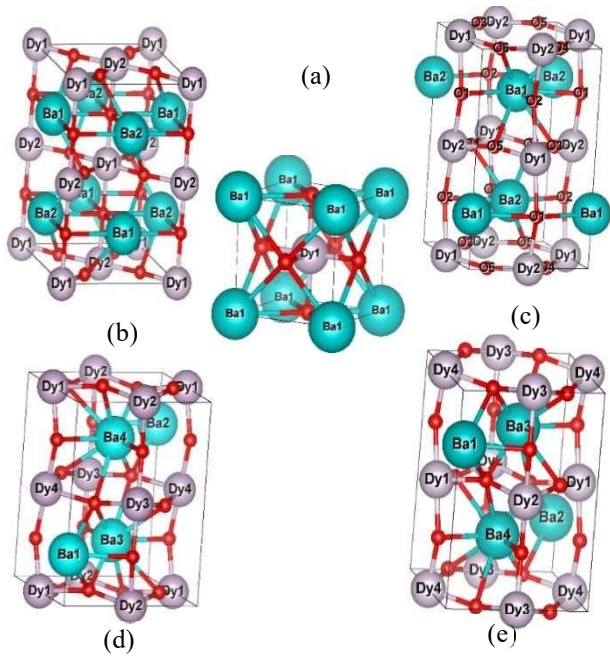
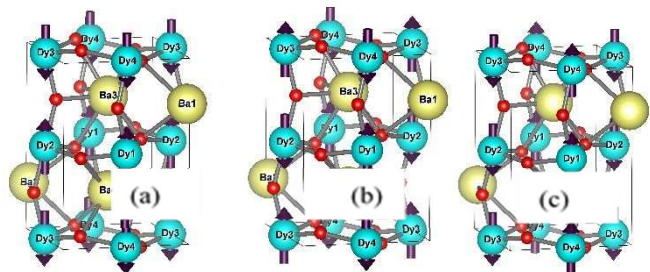


Figure 1. Crystal structure of BaDyO3 (a) cubic (pm-3m)

3.2. Magnetic stability

The magnetic stability of this material BaDyO3 is investigated using a DFT calculation to define the most favorable structure respecting the total energy of the system. BaDyO3 crystallize in orthorhombic structure with pbnm space group, in order to explore the electronic and magnetic orders in the ground state, we compare the total energy of BaDyO3 in different magnetic phase with respect to the Non-magnetic (NM) (paramagnetic) state. The calculations are made for non-spin-polarized case and ferromagnetic (FM), antiferromagnetic in the stacked plane ferromagnetic in the direction of c (AFM-C), antiferromagnetic in three directions (AFM-G) and ferromagnetic ab



antiferromagnetic planes stacked along the c-axis (AFM-A) (fig.3-b). the volume of BaDyO₃((a), (b), (c), (d), structural stability).

Table 1: Calculated resultants equilibrium lattice parameters: a [Å], b [Å], c [Å], bulk modulus B (GPa), its pressure derivative (B') and the Volume of cell [Å³] of orthorhombic BaDyO₃ obtained with LSDA and indfd3 approximations.

		BaDyO ₃	Present work	
LSDA	Cubic (#Pm3m)	Lattice constant (A°)	4,2215	
		E ₀	-41036,455658	
		B	135,140	
		B'	4,317	
		V _o	507,696	
	Tetragonal #I4/mcm	E ₀	-82072,870209	
		B	137,664	
		B'	4,623	
		V _o	1009,054	
		Orthorhombic #Ibmm	E ₀	-82072,765106
	B		120,803	
	B'		4,173	
V _o	1039,554			
Orthorhombic #pbmm	E ₀		-164145,8222365	
	B	134,339		
	B'	4,387		
	V _o	2019,594		
	Orthorhombic (# pmma)	a(A°)	11,33	
b(A°)		15,96		
c(A°)		11,15		
E ₀		-164145,710633		
B		132,955		
B'		5,077		
V _o		2015,123		
indfd3		Orthorhombic (# pmma)	a(A°)	11,39
			b(A°)	16,01
			c(A°)	11,20
	E ₀	-164147,040157		
	B	141,222		
	B'	3,295		
	V _o	2044,3871		
	E ₀ A-AFM	-164147,051488		
E ₀ C-AFM	-164147,058975			
E ₀ G-AFM	-164147,068613			

The calculated results are listed in Table 1 and illustrated in Figure 2. Note that the total energy of the AFM-G phase is the lowest, which is consistent with the theoretical results obtained for BaTbO₃[19].

3.3. Electronic band structure and density of states

Self-consistent field calculations are performed in order to study the electronic properties of BaDyO₃ in orthorhombic phase. We calculated the band structures of BaDyO₃ along the high symmetry axes in the first Brillouin zone by using the following approaches LSDA, LSDA+ U

Figure 3-a. The crystal structure with all the magnetic moments of Dy in three antiferromagnetic ordering configurations (b-d) in orthorhombic BaDyO₃: (a) AAFM, (b) C-AFM and (c) G-AFM. The arrows indicate

magnetic moment orientations on Dy atom.

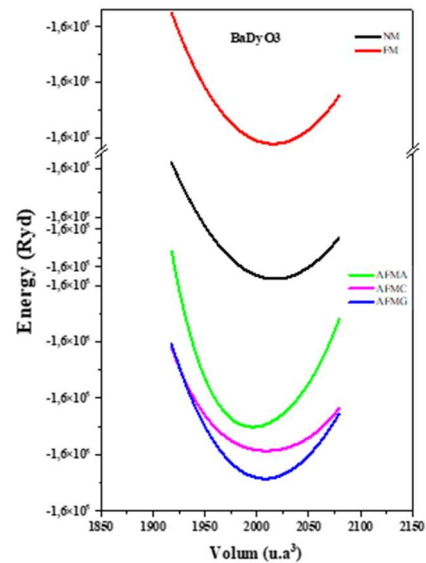


Figure 3-b. The variation of the total energy as a function of the volume of BaDyO₃(magnetic stability) and mBJ with the inclusion of different Coulomb interaction U (U = 0, 2, 4, 6 and 8eV) in the GAFM phase.

In the antiferromagnetic phase, the band structures on spins up are identical to those obtained for the towers down. Only the band structures for a spin are represented in Figure .4

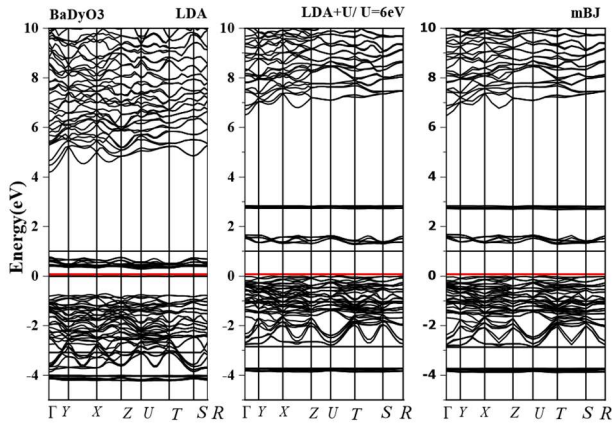


Figure 4. Band structures of BaDyO₃ within LSDA, LSDA+U and mBJ approximation.

The zero of energy is chosen to coincide with the Fermi level. Using the LSDA, we show that the band structure of BaDyO₃ (figure.4) has a semiconductor behavior because of the polarization of Fermi level in the majority spin electrons and minority one. However, the LSDA+U show a semiconductor too. The bottom of the conduction bands and the top of the valence bands are at the Γ point in the Brillouin zone which confirms that BaDyO₃ has a direct band gap with a value of 1.4eV in the minority spin electrons. We can deduct from these results that the U Hubbard correlation influences the positions of the electronic states (Dy-4f).

Generally, the LSDA+U give a wider band gap than LSDA. We can see from the figures that the energy gap increases by applying the Coulomb interaction U=2 to U = 6 eV when the state of Dy 4f is located and we introduce mBJ approximation since it gives a very close experimental gap[20], and because we do not have results calculated on this material.

The electronic structures of BaDyO₃ are studied in the antiferromagnetic phase G (G-AFM) (Fig.5) using the standard LSDA in order to compare with those from LSDA+U and mBJ.

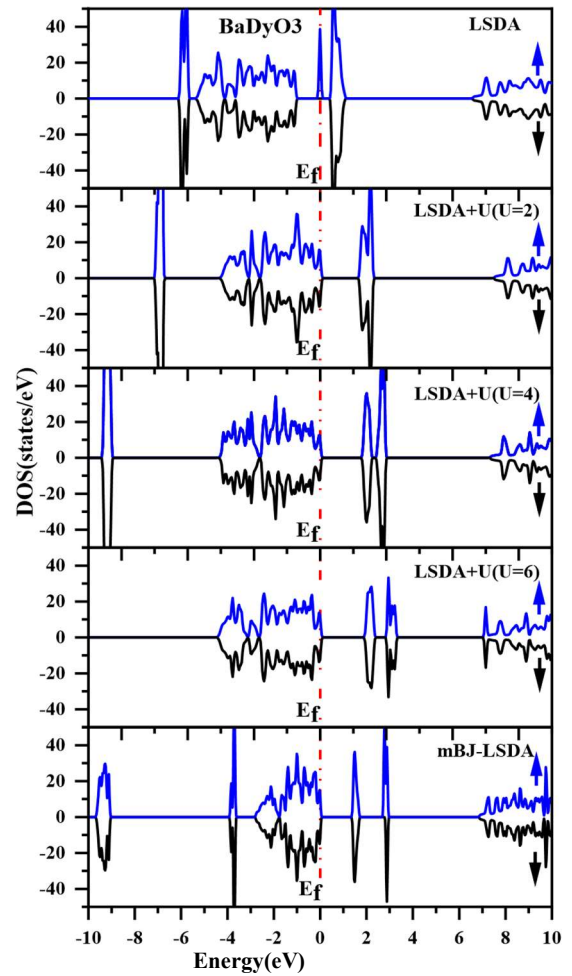


Figure 5. Total densities of states of BaDyO₃ within LSDA, LSDA+U and mBJ approximation.

The total density of states for BaDyO₃ in the spin up and down obtained using LSDA, LSDA + U and mBJ is shown in Figure 5, with U being 2.0, 4.0 and 6.0 eV. The total and partial density of states obtained using LSDA +U (U=6) and mBJ-LSDA approximations is shown in Figure 6. It is clear from the figure 6 that Ba 5p, 5d, 4f is deeply occupied at -3.0 eV and Ba 5d, 4f are all unoccupied above 5.0 eV. One can see that the valence band near E_f level is mainly contributed by O 2p. The sharp peaks around -5.0 eV is due to the hybridization of O 2p and Dy 4f, and the peak at 1.79 eV is due to unoccupied Dy 4f. The peaks from -5 to 2.5 eV originate from mixed unoccupied Dy 4f and O 2p states. From Figure.5 one can see that with the increase of U, the Dy 4f states mainly move apart from the Fermi level significantly, which move down wards slightly. Thus we suggest the Coulomb interaction U of Dy in BaDyO₃ should be chosen as 6.0 eV. Up to now, there are very few works that treat the localized f orbital's by using the LSDA + U method The optimized value Hubbard U obtained in this work is chosen in a way that the gap calculated by the mBJ

approximation coincided with that obtained by the LSDA+U.

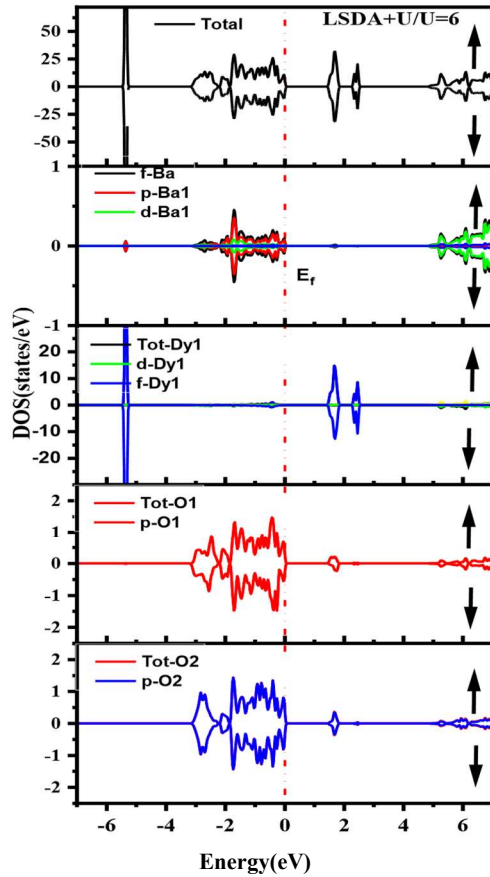


Figure 6. Total and partial densities of states of BaDyO₃ within LSDA+U approximation.

3.4 Magnetic properties

We have investigated in this part of paper; the magnetic properties of BaDyO₃ are investigated in orthorhombic phases. The stable magnetic state is evaluated by calculating the total ground state energy versus volume per unit cell for the paramagnetic, ferromagnetic, A, C and G-type anti-ferromagnetic states. The calculated ground state energy per unit cell is presented in Table 1. It is clear from the table that the stable magnetic state of the compound is G-type anti-ferromagnetic for which the ground state energy of BaDyO₃ is lower as compared to the paramagnetic and ferromagnetic states. To find the spin effect on this material, we examined especially the magnetic moment in all atoms that formed our compound using LSDA, LSDA+U and mBJ approximations. The results are resumed in Table.2.

Table 2: Calculated magnetic moments in Bohr Magneton (μ_B) For Several Sites of the orthorhombic BaDyO₃ with:

LSDA, LSDA+U and mBJ Approximations.

	LSDA	LSDA+U	mBJ
E_g (eV)	0.35	1.37	1.47
μ_{Dy}	5.235	5.436	5,229

The total magnetic moment which includes the contribution from the interstitial region arises from the Dy³⁺ ions (CsDy f: Dy³⁺) [16] with a small contribution of O sites in both approximations. For LSDA+U calculations, the total magnetic moment of the compound is 5.537 μ_B . There are two possible exchanges, one is double-exchange and the other one is super exchange [21]. Generally, double exchange is ferromagnetic and super exchange is anti-ferromagnetic. So, we suppose that the double exchange mechanism is responsible for the ferromagnetism observed in orthorhombic BaDyO₃ perovskite.

3.5 Optical properties

The study of optical properties of these materials provides useful information regarding their application in the optoelectronic devices. As BaDyO₃ has a semiconducting small band gap nature, so it is predicted that it will be an efficient compound for optoelectronic devices.

Fig. 7 shows the calculated curves of the complex dielectric function (the real and imaginary parts), absorption coefficient, reflectivity, energy loss function, refractive index, extinction coefficient (Fig. 8, Fig. 9), and optical conductivity are calculated in both the phases using LDA+U at U=4 eV using OPTIC package [22] implanted in WIEN2K in the range of 0–40 eV. All the three polarization directions (E//x, y, and z) are considered.

Dielectric functions are used as an investigative tool for the calculation of various optical properties of a material. In Fig. 7, the real part of dielectric function $\epsilon_1(\omega)$ is plotted for both orthorhombic crystal structures. From the figure it can be seen that it has a negligible anisotropy.

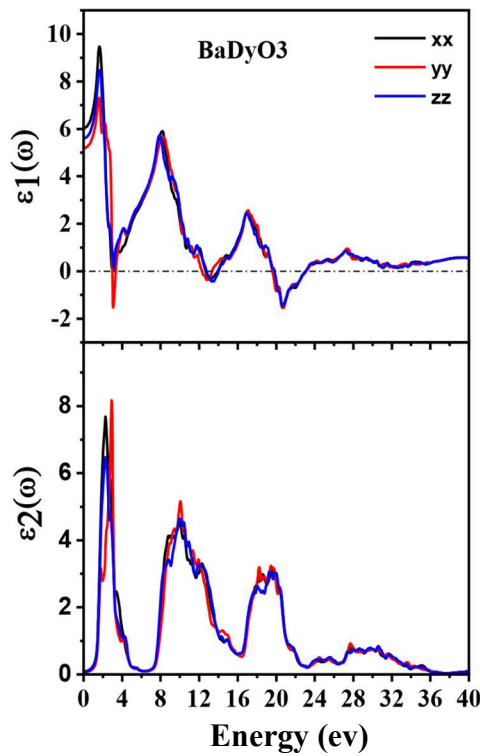


Figure 7. The real and imaginary part of dielectric function for BaDyO3.

The electronic polarizability of a material can be understood from the real part of the dielectric function

$\epsilon_1(\omega)$ [Fig. 7]. The static dielectric constant $\epsilon_1(0)$ along the three crystallographic directions is found to be 5.2 for E//x, 5.6 for E//y, and 6.0 for E//z, respectively.

It has three peaks and these peaks correspond to different optical transitions. The first peak is observed at 1.6 eV and the second at 8.04 eV the third at 17.07 eV.

The real part of dielectric function becomes negative for energies larger than 20 eV which means that the compound shows metallic behavior.

The imaginary part of dielectric function $\epsilon_2(\omega)$ is shown in 7. The offset points in all optical axes are observed at 1.37 eV which corresponds to the optical gap of the compound.

A wide range of absorption region is observed with two main peaks. The first peak is obtained at 3.41 eV for all the axes while the second one at 7.04 eV. As the material has wide and direct band gap nature, it could be efficient candidate for visible optoelectronic applications.

The average value of the zero-frequency dielectric constant $\epsilon_1(0)$ is 5.6. However, there is no experimental polarized zero frequency dielectric constant available for comparison. These results clearly indicate anisotropy in the optical properties of orthorhombic BaDyO3.

From the zero-frequency limit, they start increasing and reach the maximum value of 9.42 at 1.76 eV for E//x, 8.53 at 1.86 eV for E//y, and 7.44 at 2.00 eV for E//z, respectively.

The imaginary part $\epsilon_2(\omega)$ Fig. 7 gives information of the absorption behavior of BaDyO3. The threshold energy of the dielectric function is at 1.37 eV, in good accordance with the fundamental gap. The obtained optical gap once again proves that LDA+U can provide an accurate band gap for magnetic semiconductors.

The imaginary part $\epsilon_2(\omega)$ Fig. 7 indicates that BaDyO3 is anisotropic and its maximum absorption peak values are around 2.7, 2.89 and 2.43 eV for E//x, E//y and E//z, respectively. From Fig. 7, for the imaginary part $\epsilon_2(\omega)$, it is

clear that there are strong absorption peaks in the energy range of 1.5–22 eV. Because $\epsilon_2(\omega)$ is related to the DOS, these peaks reflect some transitions between different orbitals. Compared with Fig. 6, it can be recognized that the peaks around 3.5–4.5 eV are mainly due to transitions from Dy-4f valence bands to O-2p conduction bands.

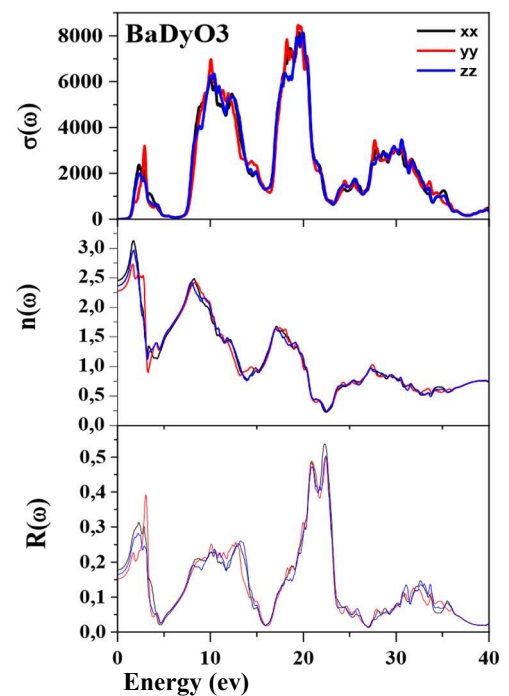


Figure 8. Optical conductivity, refractive index and the reflectivity of BaDyO3

The calculated refractive index $n(\omega)$ for BaDyO3 in the energy range 0–40 eV is plotted in Fig. 8. From the figure The static refractive index $n(0)$ is found to have the value 2.46 for E//x, 2.28 for E//y, and 2.36 for E//z, respectively.

The average value of $n(0)$ is equal to 2.37. The maximum refractive index is found in the direct transition from the valence band to conduction band. After this peak value the refractive index decreases with respect to higher energies, this is due to the fact that higher energy photons are absorbed by the material and the material becomes gradually opaque.

The reflectivity coefficient $R(\omega)$ is calculated for BaDyO₃ and shown in Fig. 8, the zero-frequency reflectivity values are 17.8% for E//x, 15.2% for E//y, and 16.4% for E//z, respectively. The maximum reflectivity values are about 53.7, 49.7 and 49.3%, which occurs at 22.2 eV for E//x, 22.4 eV for E//y and E//z, respectively. Interestingly, the strong reflectivity maximum between 15 and 23.3 eV originates from the interband transitions.

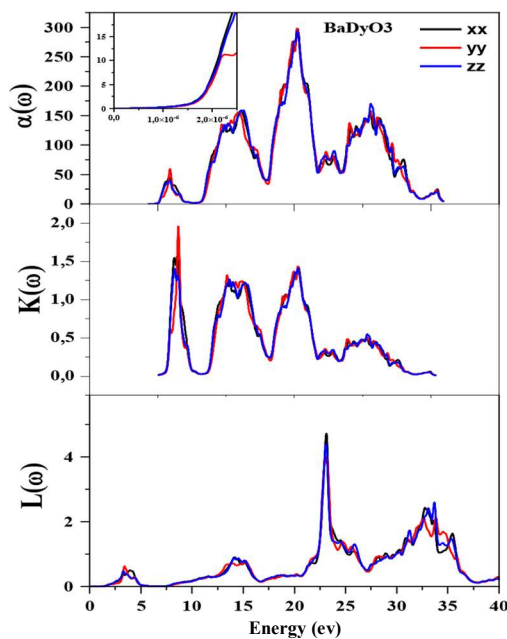


Figure 9. Absorption coefficient $\alpha(\omega)$, Energy loss function $L(\omega)$, Extinction coefficient $k(\omega)$ of BaDyO₃.

The energy loss function $L(\omega)$ for BaDyO₃ is plotted in Fig.9. It is obvious from the figure that for a photon with energy less than the band gap of a material no energy loss occurs, which means no scattering happens. It is observed in the range of energy 22-25eV and 30-35eV that the energy loss is maximum, where there are two peaks at 23.14eV and 32.83eV. This peak in the energy loss spectrum corresponds to the plasma resonance.

The extinction coefficient $k(\omega)$ reflects the maximum absorption in the medium at 1.50 eV for E//x, 3.60 eV for E//y, and 1.04 eV for E//z, respectively.

The optical conductivity $\varsigma(\omega)$ is shown in Fig. 9. It starts from 1.37 eV and has similar features with the absorption coefficient $\alpha(\omega)$ in Fig. 8.

4. Conclusion

The electronic structures of BaDyO₃ have been studied by using LSDA, LSDA+U and mBJ methods.

By calculating the total energies of NM, FM, A-AFM, C-AFM and G-AFM BaDyO₃, the ground magnetic phase of the compound is found to be G-AFM with the lattice's constant of $a=11.39 \text{ \AA}$, $b=16.01 \text{ \AA}$ and $c=11.20 \text{ \AA}$.

The inclusion of Hubbard U of Dy ions gives significant effects on the electronic density of states, energy band structure, and the magnetic moment. The optimized value of U in BaDyO₃ is suggested to be 6.0 eV from our calculation. The energy band of BaDyO₃ is found to be direct with a gap of 1, 4eV. Optical properties show that the material is active in visible region.

References

- [1] J. G. Bednorz, K. A. Müller, Phys. Rev. Lett. 52 (1984) 2289.
- [2] H.F. Li, G.H. Zhang, Yue Zheng, Biao Wang, W. J. Chen, Acta Materialia 76 (2014) 472-481
- [3] https://ieeexplore.ieee.org/ielx5/58/32256/01503988.pdf?tp=&arnumber=1503988&isnumber=32256&ref=s_3 (2013) 61.
- [4] Z. Xing, H. Wang, B. Xu, G. Ma, Y. Huang, J. Kang, L. Zhu, Materials Design.ens 62 (2014) 57-63.
- [5] B. Deka, S. Ravi, A. Perumal, D. Pamu, Physica B Condens. Matter 448 (2014) 204-206.
- [6] D. Zhu, P. Cao, W. Liu, X. Ma, A. Maignan, B. Raveau, Mater. Lett. 61(2007) 617-620.
- [7] J. Panda, S. K. Giri, T. Nath, IOP Conf. Ser.: Mater. Sci. Eng. 73 (2015) 012134.
- [8] G. Banach and W. M. Temmerman, Phys. Rev. B 69, (2004) 054427.
- [9] A. Labdelli, S. Meskine, A. Boukourt, R. Khenata, J. New Technol. Mater Vol. 08, N°01 (2018)126-138.
- [10] K. Schwarz, P. Blaha, Comput. Mater. Sci. 28 (2003) 259-273.
- [11] P. Blaha, K. Schwarz, G. Madsen, wien2k. An augmented plane wave local orbitals program for calculating crystal properties (2001).
- [12] O. Krogh Andersen, Phys. Rev. B 12 (1975) 3060.
- [13] W. Kohn, L. J. Sham, Phys. Rev. 140 (1965) A1133.
- [14] J. P. Perdew, Y. Wang, Phys. Rev. B 98 (2018) 079904.
- [15] V. I. Anisimov, O. Gunnarsson, Phys. Rev. B 43 (1991) 7570.
- [16] F.D. Murnaghan, Proc. Natl. Acad. Sci. 30 (1944) 244-247.

- [17] H.C. Froelich, U.S. Patent 2 392 (1946) 814.
- [18] C. Ma, L. Ye, Z. Yang, J. Phys. Condens.17(2005) 7963.
- [19] Z. Ali, I. Ahmad, S.J. Asadabadi, Comput. Mater. Sci. 67 (2013)151-155.
- [20] J. A. Camargo-Martínez, R. Baquero, cond-mat.str-el 1208 (2012) 2057.
- [21] S. Blundell, D. Thouless, J. Magn. Mater. (2001) Oxford university press New York.
- [22] C. Ambrosch-Draxl, J. A. Majewski, P. Vogl and G. Leising, Phys. Rev. B 51 (1995) 9665.